RSC Advances

ROYAL SOCIETY OF CHEMISTRY

www.rsc.org/advances

RSC Advances

Paper

Highly flexible, tailorable and all-solid-state supercapacitors from carbon nanotube-MnO_x composite films

Received 00th August 2015,
Accepted 00th January 20xx

DOI: 10.1039/x0xx00000x

www.rsc.org/

F. M. Guo, R. Q. Xu, X. Cui, X. B. Zang, L. Zhang, Q. Chen, K. L. Wang and J. Q. Wei*

Carbon nanotube (CNT) films are promising materials for constructing highly flexible composite for supercapacitor electrodes. Here, we prepared composite films with sandwich structure and outstanding electrochemical properties by electrodepositing manganese oxide (MnO_x) to the flexible CNT macrofilms. All-solid-state supercapacitors were then fabricated from the CNT-MnO_x composite films using poly(vinylalcohol)-potassium hydroxide as gel electrolyte. The supercapacitors have high performance with a specific capacitance of 73.4 F/g and an energy density of 6.2 Wh/kg. The supercapacitors also exhibit high flexibility and stability under bending and kneading. When cut into small parts, the supercapacitor fragments can still work independently. The highly flexible and tailorable supercapacitors have great potential in the flexible electronics in the future.

1. Introduction

Flexible and portable electronic devices, such as electronic skins, bendable displays and touching screens, wearable solar battery, and supercapacitors,[1-5] have promising applications in the future. As an energy storage device, supercapacitor can store energy and supply power to the electronics due to their high power density, fast charge-discharge ability, and long cycle life. According to the charge storage mechanism, the supercapacitors can be classified as electric double layer capacitors (EDLCs) and pseudocapacitors. Charge separation occurs at the electrode-electrolyte interface for the EDLCs, while redox reactions occur in pseudocapacitive electrodes.[6] For the potential applications in the flexible devices, it requires the supercapacitors not only to have high specific capacitance and energy density, but also to be flexible. Recently, flexible all-solid-state supercapacitors have attracted extensive attentions because they can provide not only excellent capacitive behaviours as those of conventional supercapacitors, but also have advantages in adaptability, lightweight, and portability.[4,5,7] These all-solid-state supercapacitors generally consist of flexible electrodes, gel electrolytes, a separator, and a flexible substrate. The flexibility of the supercapacitor were demonstrated by bending, twisting, winding, and even weaving. However, the flexible electronics might suffer severer deformation, or even mechanical damage. The flexible supercapacitors are also required to have high reliability when they are seriously deformed, and even accidentally cut. [8]

The electrodes with high electrochemical properties hold a key to fabricate high quality flexible supercapacitors. Carbonaceous materials, including activated carbon, carbon nanotubes (CNTs), graphene, and so on, have been widely investigated as electrodes in the flexible supercapacitors.[4,5,9-20] Among these carbonaceous materials, CNTs with various assemblies, including powder, fibers and films, have been extensively investigated in the flexible supercapacitors owing to their outstanding properties, such as high electrical conductivity, chemical stability, mechanical properties, and large activated surface areas.[5,9,10,14-19] However, the pure CNTs suffer from relative low specific capacitance due to the relative low specific surface area and EDLC energy storage mechanism. On the other hand, transition metal oxides, such as manganese oxide (MnO_x), have high theoretical pseudocapacitance, but very low electrical conductivity.[20-22] It might take the advantages of the high conductivity and flexibility of CNTs and high pseudocapacitance of MnO_x to prepare hybrid electrodes from CNTs and MnO_x, where CNTs act as conducting channel and scaffold for loading MnO_x.[23-27]

Key Lab for Advanced Materials Processing Technology of Education Ministry; State Key Lab of New Ceramic and Fine Processing; School of Materials Science and Engineering, Tsinghua University, Beijing 100084, P.R. China
E-mail: jqwei@tsinghua.edu.cn; Tel: +86-10-62781065

Here, we prepared flexible CNT-MnO_x composite films with excellent electrochemical properties by electrodepositing MnO_x on the CNT macrofilms, and fabricated all-solid-state supercapacitors basing on the composite films. The supercapacitors shows high flexibility and stability under bending and even kneading. The composite supercapacitors can be cut into pieces which can work independently. We also demonstrated potential applications of the supercapacitors in powering a stopwatch and a LED light.

2. Experimental

Preparation of CNT-MnO_x composite films

Large area CNT macrofilms were fabricated by an improved floating catalyst chemical vapour deposition method which have been described in details in our recent reports.[19,28] During the growth of CNTs, xylene solution containing small amount of ferrocene and sulphur was atomized and fed into a quartz reactor. Stockings-like CNT thin films were blown out from the reactor continuously and collected by a wheel rotating perpendicularly to the gas flow, which formed macroscopic CNT films. The CNT macrofilms were purified by immersing in H_2O_2 (30 wt%) solution for 72 hrs and then in HCl (37 wt%) solution for 12 hrs to remove the impurities of amorphous carbon and metallic catalyst particles. After purification, the CNT films were washed in deionized (DI) water for several times and then dried at 80℃ for 1 h. The purified CNT films were cut into small pieces with desired dimensions (typically 1×1 cm).

The CNT-MnO_x composite films were prepared by an electrodeposition method in aqueous solution consisting of 10 mM $MnSO_4$ and 100 mM Na_2SO_4 at a constant potential of 1 V, where a purified CNT film was used as the working electrode, a Ag/AgCl was used as the reference electrode, and a Pt foil was used as the counter electrode, respectively.[20, 28] After electrodeposition, the composite film was cleaned with DI water to get rid of residual solution and dried in an oven at 80℃ for 1 h. The content of the MnO_x in the composite film was calculated by measuring the weight gain before and after electrodeposition.

Fabrication of CNT-MnO_x supercapacitors

All-solid-state supercapacitors were fabricated by coating the CNT-MnO_x composite films with poly(vinylalcohol)-potassium hydroxide (PVA-KOH) gel electrolyte (containing 1 g PVA , 0.56 g KOH and 10 mL DI water) for several times,[16] and then carefully placing the two CNT-MnO_x film electrodes on top of each other on a flexible polyethylene terephthalate (PET) or a polyethylene (PE) ceiling film.

Characterization

The CNT-MnO_x composite films were characterized by using scanning electron microscopy (SEM, LEO 1530), X-ray diffraction (XRD, SmartLab) and X-ray photoelectron spectroscopy (XPS, 5300ESCA), respectively. The electrochemical properties of the CNT-MnO_x composite electrodes and supercapacitors were tested by using a chemical workstation (CHI 660E, Shanghai Chen Hua Co., Ltd, China), respectively. For the CNT-MnO_x electrodes, cyclic voltammetry curves (CV), galvanostatic charge-discharge (GCD) behaviours, and electrochemical impedance spectroscopy (EIS) were measured by using a three-electrode system in 0.5 M Na_2SO_4 aqueous electrolyte, where the CNT-MnO_x composite films were used as the working electrode, a Ag/AgCl was used as the reference electrode, and a Pt foil was used as the counter electrode. For the all-solid-state CNT-MnO_x supercapacitors, the capacitive properties were measured by a two-electrode method.

Calculation method

For the electrodes, the capacitances are calculated from CV curves by the equation of $C = \int IdV/vV$, where, I is the response current, V is the potential window and v is the scan rate. The areal specific capacitance C_a=C/S and the mass specific capacitance is C_s= C/m, where S is the area of the film, m is the mass of the electrode.

For the supercapacitors, the capacitances C, energy density E and power density P are calculated from GCD curves using following equations: C= $I/(\Delta V/\Delta t)$=$I\,\Delta t/\Delta V$; C_s= $C/(m_1+m_2)$; $E=C_s\Delta V^2/2$; $P=E/\Delta t$; where, m_1 and m_2 are the mass of the two electrodes of the supercapacitors, C_s is the mass specific capacitance, I is the discharge current, Δt is the discharge time, ΔV is the voltage window during the discharge process after IR drop, respectively.

3. Results and discussion

After purification, the CNT films still maintain the macroscopic structure. Fig. 1a shows an optical image of a purified CNT macrofilm with 3.5 cm in width and more than 25 cm in length. The

thickness of the film is several to tens of microns depending on the growing time of CNTs. The macrofilm consists of large amount of long and entangled CNT bundles which interweave with each other and form an unwoven film.[19,28] The purified CNTs are very clean under SEM observation, which indicates that most of the catalyst particles are removed from the film. (see Fig. S1a). The macrofilms mainly consist of single-walled and double-walled CNTs with diameter of 2~3 nm (see Fig. S1b).Thermal gravimetric analysis curve shows that there are still ~9 wt% Fe catalyst in the samples (see Fig. S1c). The CNT films have low sheet resistances of only about 0.5~1 Ω sq^{-1}. The purified CNT film can be bent, crumpled into a ball, and even twisted (see supporting information of Fig. S2 and Video S1). The twisted CNT films can also recover to its original state. It provides a tough and highly flexible substrate for making a flexible composite film.

Manganese oxide are deposited on the purified CNT films by an electrodeposition method, forming CNT-MnO_x composite films. The content and distribution of the MnO_x depend on the deposition time. Figs. 1b to 1e show some SEM images of the CNT-MnO_x composite prepared at different deposition times. At the beginning of deposition (deposition time: 100 s), MnO_x nanoflowers deposit and distribute randomly on the surface of the CNT film (Fig. S3a). The nanoflowers, containing many nanoflakes (see Fig. 1 b), have uniform diameters ranging from 200 to 600 nm. As the deposition time extends to 300 s, the density of the nanoflowers on the surface of CNT film increases significantly, but the dimensions of the nanoflowers almost maintain unchanged (see Fig. S3b). It is clear from Fig. 1c that the MnO_x nanoflowers deposit on the CNT bundles or are wrapped by the CNT bundles, which makes the MnO_x contact with the CNT films tightly. Within the composite, the long CNT bundles form a conductive network for the MnO_x nanoflowers.[11] When the deposition time reaches 600 s, the CNT films were almost fully covered by a continuous film of the MnO_x nanoflowers from both sides (Fig. 1d and Fig. S3c). After that, the MnO_x deposit among the MnO_x nanoflowers and form a uniformed layer of MnO_x nanoflakes (Fig. 1e and Fig. S3d). The loading of MnO_x in the composite increases as the deposition time extends, which ranges from ~62 to ~95 wt% for the deposition time varies from 100 s to 2400 s (see supporting information of Table S1). It is noted that the MnO_x deposit on the both surfaces of the CNT film, which indicates that the CNT-MnO_x composite have sandwich structure when the CNT film is fully covered by MnO_x.

The composites with proper surface area and suitable pore size distribution are favourable for using as electrode materials. The specific surface area of the CNT-MnO_x composite films were measured by using the Brunauer-Emmett-Teller (BET) method and the corresponding pore size distribution was obtained by employing the Barrett-Joyner-Halenda (BJH) method (see Fig. S4). The purified CNT film has moderate specific surface area of 159.4 m^2/g, and a broad pore size distribution from 4 to 90 nm. The CNT-MnO_x films prepared at deposition time of 600, 1200 and 2400 s have specific surface area of 156.7, 154.6 and 140.9 m^2/g (Fig. S4a), and average pore size of 9.9 nm, 3.9 nm and 3.8 nm (Fig. S4b), respectively. The specific surface area of the CNT films decrease slightly after deposition of MnO_x, but the pore size distribution decreases and narrows significantly. The CNT-MnO_x composite films still have abundant pores for electrolyte in the supercapacitors.[21]

X-ray diffraction (XRD) and X-ray photoelectron spectroscopy (XPS) spectra are used to determine the structure and the state of the MnO_x. There are three evident peaks centred at 38°, 44.3° and 64.5° in the XRD patterns of the CNT-MnO_x composite, respectively (Fig. 2a). These peaks do not fit with the crystalline structure of either MnO_2 or Mn_2O_3 quite well.[21,25,29] The Mn 2p XPS spectrum in Fig. 2b shows two prominent peaks centred at 642.2eV and 653.9eV, corresponding to the binding energy of Mn $2p_{3/2}$ and Mn $2p_{1/2}$, respectively. It indicates that the manganese element has various band structure according to the Mn 2p spinning energy (11.8eV).[26, 27, 30] It implies that the manganese oxide here is a non-stoichiometric compound of MnO_x.[17]

The electrochemical properties of the CNT-MnO_x composite films are measured by using a three-electrode setup in 0.5 M Na_2SO_4 electrolyte. Fig. 3a shows a CV curve of the CNT-MnO_x composite film prepared by 1200 s deposition. It has good rectangle shape. For comparison, we also measure the electrochemical properties of a purified CNT film at the same conditions. The areal capacitance of the CNT-MnO_2 composite electrode reaches 174 mF/cm^2 (173.7 F/g) at 10 mV/s and the purified CNT film was about 5 mF/cm^2 (17.3 F/g) at scan rate of 10 mV/s. The increase of the areal capacitance of the CNT-MnO_x composite derives from the pseudocapacitance of the MnO_x.[20, 27, 30] The impedance spectra are

tested in the frequency range of 0.01 to 1M Hz. The Nyquist plots in Fig. 3b show that the curve of the CNT-MnO_x is almost vertical to the imaginary axis at low frequency region, while the purified CNT film shows a finite slope. From the high frequency range, the equivalent series resistance (ESR) is 7.7 Ω for the CNT-MnO_x film electrode, while it is 6 Ω for the purified CNT electrode (inset of Fig. 3b). The interface charge transfer resistance (R_{ct}) of the CNT-MnO_x composite film from the semicircle is 4.5 Ω, which is lower than that of CNT film (5.8 Ω). The relative low R_{ct} of the CNT-MnO_x derives from enhance of affinity with the Na_2SO_4 electrolyte. Nyquist plots and Bode plots (Fig. S5 and Table S2) of composites at different deposition times show that, R_{ct}, high frequency resistance (HFR) and time constant increase as the deposition time increase. Fig. 3c shows the CV curves of the CNT-MnO_x electrode at various scan rates. The CV curves of the CNT-MnO_x composite have nearly rectangular shapes at scan rates ranging from 10 to 100 mV/s, showing a good capacitance retention. The composite electrode also has good linearity and symmetry from 0.5 to 5 A/g in the GCD curves (Fig. 3d). The CNT-MnO_x electrodes are stable in the cycling CV test (Fig. 3e). It shows that the electrode had retained 97.9% of the original specific capacitance after 10000 cycles at 100 mV/s. The CV curves of the 1000^{th} and 10000^{th} test almost overlap with that of the original test (see inset of Fig. 3e).

Because of its high specific capacitance and very low conductivity, MnO_x in the composite impact the electrochemical properties from two aspects: improving capacitance and reducing capacitance retention rate. Fig. 3f shows the plots of the areal capacitances depending on the deposition time of MnO_x at various scan rates. It is clear that the areal capacitance of the CNT-MnO_x composite electrode increases significantly as the deposition time prolongs, due to increase of the content of MnO_x. The areal capacitance reaches to 366 mF/cm^2 at a deposition time of 2400 s at 5 mV/s, which is twice as high as that with a deposition time of 1200 s (185 mF/cm^2). This is owing to the psuedocapacitance of MnO_x loaded on the composite electrodes. On the other hand, the capacitance retention rate decreases evidently as the deposition time prolongs. The capacitance retention rate (see Fig. S6) is about 68% when the scan rate increases from 5 to 50 mV/s for the electrode with a deposition time of 1200 s, but it drops to only 54% for the electrode with a deposition time of 2400 s because of the low electrical conductivity of MnO_x.

We also provided the CV curves of the CNT-MnOx electrodes prepared at various deposition times in Fig. 4. The CV curves remain good rectangular shape for the samples prepared with deposition time of 300 and 600 s (Fig. 4a and b), but the CV curves deviate severely from the rectangular shape for the electrode with deposition time of 2400 s (Fig. 4c). These CV curves indicate that the resistances of the electrode increase as deposition time prolongs, resulting in poor electrical conductivity and capacitive properties. By combining consideration of areal capacitance and capacitance retention rate, we choose 1200 s as the best deposition time.

We fabricate symmetric and all-solid-state supercapacitors on flexible PET substrates by using the CNT-MnO_x composite films as electrodes, and PVA-KOH gel electrolyte as binders and separators. The electrochemical performances of the supercapacitors are similar to those of the electrodes in aqueous electrolyte. Fig. 5a is the CV curves of a CNT-MnO_x supercapacitor, showing good rectangular shapes at scan rates ranging from 10 to 100 mV/s. The GCD curves in Fig. 5b also shows good triangle shape for current density varying from 0.5 A/g to 4 A/g, showing a relative low ESR of the supercapacitor. The supercapacitor has high performance with a high specific capacitance of 73.4 F/g (corresponding to 293 F/g for electrode), an energy density of 6.2 Wh/kg, and a power density of 0.2 kW/kg at 0.5 A/g, respectively. At high current density of 4 A/g, the supercapacitor still has a specific capacitance of 50.9 F/g, an energy density of 2.8 Wh/kg, and a power density of 1.3 KW/kg. The energy density and power density are close to the best values reported previously.[16, 31-33] The Nyquist plot shows that the device has an ESR of 12.4 Ω at high frequency (inset of Fig. 5c) and a line with a finite slope at low frequency (Fig. 5c), which indicates a low diffusive resistance for cation intercalation/de-intercalation.[34] The supercapacitor is also very stable during the cyclic test. The capacitance has 90.4% retention after 1000 cycles during cyclic voltammetry test at 200 mV/s (see Fig. 5d).

The CNT-MnO_x supercapacitor also exhibits good flexibility and reliability under bending. Fig. 6a shows CV curves of a supercapacitor on a 50 μm thick PET substrate being bent to series of angles (0°, 30°, 60° and 90°). These CV curves at bending angle of 30°, 60° and 90° almost overlap with each other. But the capacitance increases slightly when compared with the original state (0°), which might derive from the improvement of contact

between the electrodes and electrolyte under pressure. Actually, the supercapacitor possibly undergoes deformation more than bending and curling. It might be folded, or even kneaded.[4, 8] Fig. 6b shows the CV curves of a CNT-MnO_x supercapacitor (5 cm^2 in area) on a PE ceiling film substrate. The supercapacitor can be kneaded into a ball, and then flattened to the original state (recovered) for several times. The CV curves under kneading and flattening almost maintain unchanged at high scan rate of 200 mV/s. This shows that the supercapacitor is highly flexible and stable under large deformation. The high flexibility of the supercapacitor is owing to sandwich structure of the composite film, where MnO_x distribute homogenously on the strong, tough, and highly flexible CNT macrofilms.

Besides high flexibility, the supercapacitor also shows excellent reliability by cutting. Fig. 6c shows a supercapacitor being cut into two parts. The two parts of supercapactors can work well independently (see Fig. 6c and supporting information of Fig. S7). When connected in parallel, the capacitance of the combination of two parts loses slightly (91% remain). This indicates that the CNT-MnO_x composite film has stable and uniform structure which can be cut into pieces.

In order to meet the energy and power demands, sometimes, the supercapacitors are connected in series and/or in parallel.[12] Here, we connect three supercapacitors in series to improve the voltage output (Fig. 7a). Each supercapacitor has a voltage window of 0.8 V. When they are connected in series, the operating voltage window reaches 2.4 V. The charge time was about 34 seconds at a current density of 5 mA/cm^2 and discharge time was 32 s, almost the same with that of individual supercapacitor (29.4 s). The energy density and power density of each capacitor was shown in table S3. The three supercapacitors in series could power a stopwatch for more than two minutes, or a light emitting diode for more than 30 seconds (Fig. 7b and 7c).

4. Conclusions

In summary, we prepare CNT-MnO_x composite films with high electrochemical properties by electrodepositing MnO_x on the CNT macrofilms in $MnSO_4$ and Na_2SO_4 aqueous solution. All-solid-state supercapacitors are fabricated from the flexible CNT-MnO_x composite films using PVA-KOH as gel electrolyte. The CNT-MnO_x supercapacitors have excellent capacitive properties with high specific capacitance of 73.4 F/g at 0.5 A/g. The supercapacitors are highly flexible and reliable under bending or kneading. The supercapacitors can be even cut into pieces which can work well independently. The CNT-MnO_x supercapacitors show great potentials in the flexible electronics in the future.

Acknowledgements

This work was supported by National Natural Science Foundation of China (51172122) and Shenzhen Jiawei Photovoltaic Lighting Co., Ltd.

References

1 G. Schwartz, B. C.-K. Tee, J. G. Mei, A. L. Appleton, D. H. Kim, H. L. Wang and Z. N. Bao, *Nat. Commun.*, 2013, **4**, 1859.
2 X. Lee, T. T. Yang, X. Li, R. J. Zhang, M. Zhu, H. Z. Zhang, D. Xie, J. Q. Wei, M. L. Zhong, K. L. Wang, D. H. Wu, Z. H. Li and H. W. Zhu, *Appl. Phys. Lett.*, 2013, **102**, 163117.
3 Y. H. Lee, J. S. Kim, J. Nob, I. Lee, H. J. Kim, S. Choi, J. Seo, S. Jeon, T. S. Kim, J. Y. Lee and J. W. Choi, *Nano Lett.*, 2013, **13**, 5753.
4 X. Zang, Q. Chen, P. X. Li, Y. J He, X. M. Li, M. Zhu, X. Li, K. L. Wang, M. L. Zhong, D. H. Wu and H. W. Zhu, *Small*, 2014, **10**, 2583.
5 C. Z. Meng, C. H. Liu, L. Z. Chen, C. H. Hu and S. S. Fan, *Nano Lett.*, 2010, **10**, 4025.
6 J. R. Miller and P. Simon, *Sci.*, 2008, **321**, 651.
7 D. P. Dubal, Kim, J. G. Kim, Y. Kim, R. Holze, C. D. Lokhande, W. B. Kim, *Energy. Technol.*, 2014, **2**, 325.
8 H. Wang, B. W. Zhu, W. C. Jiang, Y. Yang, W. R. Leow, H. Wang and X. D. Chen, *Adv. Mater.*, 2014, **26**, 3638.
9 X. M. Ma, L. H. Gan, M. X. Liu, P. K. Tripathi, Y. H. Zhao, Z. J. Xu, D. Z. Zhu and L. W. Chen, *J. Mater. Chem. A*, 2014, **2**, 8407
10 M. X. Liu, J. S. Qian, Y. H. Zhao, D. Z. Zhu, L. H. Gan and L. W. Chen, *J. Mater. Chem. A*, 2015, **3**, 1151
11 L. L. Zhang and X. S. Zhao, *Chem. Soc. Rev.*, 2009, **38**, 2520.
12 X. Xiao, T. Q. Li, Y. Gao, H. Y. Jin, W. J. Ni, W. H. Zhan, X. H. Zhang, Y. Z. Cao, J. W. Zhong, L. Gong, W. C. Yen, W. J. Mai, J. Chen, K. F. Huo, Y. L. Chueh, Z. L. Wang and J. Zhou, *ACS Nano*, 2012, **6**, 9200.
13 K. X. Sheng, Y. Q. Sun, C. Li, W. J. Yuan and G. Q. Shi, *Sci. Rep.*, 2012, **2**, 247.
14 Y. W. Cheng, S. T. Lu, H. B. Zhang, C. V. Varanasi and J. Liu, *Nano Lett.*, 2012, **12**, 4206.
15 D. H. Zhang, M. H. Miao, H. T. Niu and Z. X. Wei, *ACS Nano*, 2014, **8**, 4571.
16 C. Choi, J. A. Lee, A. Y. Choi, Y. T. Kim, X. Lepró, M. D. Lima, R. H. Baughman and S. J. Kim, *Adv. Mater.*, 2014, **26**, 2059.
17 J. H. Kim, K. H. Lee, L. J. Overzet and G. S. Lee, *Nano Lett.*, 2011, **11**, 2611.
18 W. Chen, R. B. Rakhi, L. B. Hu, X. Xie, Y. Cui and H. N. Alshareef, *Nano Lett.*, 2011, **11**, 5165.

19 S. Q. He, J. Q. Wei, F. M. Guo, R. Q. Xu, C. Li, X. Cui, H. W. Zhu, K. L. Wang and D. H. Wu, *J. Mater. Chem. A*, 2014, **2,** 5898.
20 L. Hu, W. Chen, X. Xie, N. Liu, Y. Yang, H. Wu, Y. Yao, M. Pasta, H. N. Alshareef and Y. Cui, *ACS Nano*, 2011, **5**, 8904.
21 W. F. Wei, X. W. Cui, W. X. Chen and D. G. Ivey, *Chem. Soc. Rev.*, 2011, **40**, 1697.
22 V. Subramanian, H. W. Zhu, R. Vajtai, P. M. Ajayan and B. Q. Wei, *J. Phys. Chem. B*, 2005, **109**, 20207.
23 H. Zhang, G. P. Cao, Z. Y. Wang, Y. S. Yang, Z. J. Shi and Z. N. Gu, *Nano Lett*, 2008, **8**, 2664.
24 Y. Hou, Y.W. Cheng, T. Hobson and J. Liu, *Nano Lett*, 2010, **10**, 2727.
25 S. L. Chou, J. Z. Wang, S. Y. Chew, H. K. Liu and S. X. Dou, *Electrochem. Commun.,* 2008, **10**, 1724.
26 J. Yan, Z. J. Fan, T. Wei, J. Cheng, B. Shao, K. Wang, L. P. Song and M. L. Zhang, *J. Power Sources*, 2009, **194**, 1202.
27 S.W. Lee, J. Kim, S. Chen, P. T. Hammond and Y. Shao-horn, *ACS Nano*, 2010, **4**, 3889.
28 R. Q. Xu, J. Q. Wei, F. M. Guo, X. Cui, T. Y. Zhang, H. W. Zhu, K. L. Wang and D. H. Wu. *RSC Adv.*, 2015, **5**, 22015.
29 L. L. Peng, X. Peng, B. R. Liu, C. Z. Wu, Y. Xie and G. H. Yu, *Nano Lett*, 2013, **13**, 2151.
30 M. Toupin, T. Brousse and D. Bélanger, *Chem. Mater.*, 2004, **16**, 3184.
31 H. Xia, J. K. Feng, H. L. Wang, M. O. Lai and L. Lu, *J. Power Sources*, 2010, **195**, 4410.
32 J. Ren, L. Li, C. Chen, X. L. Chen, Z. B. Cai, L. B. Qiu, Y. G. Wang, X. R. Zhu and H. S. Peng, *Adv. Mater.*, 2013, **25**, 1155.
33 C. Y. Guo, H. Li, X. Zhang, H. H. Huo, C. L. Xu, *Sensor Actuat. B-Chem.*, 2015, **206**, 407.
34 W. F. Wei, X. W. Cui, W. X. Chen and D. G. Ivey, J. Phys. Chem. C, 2008, **112**, 15075.

Figures and Captions

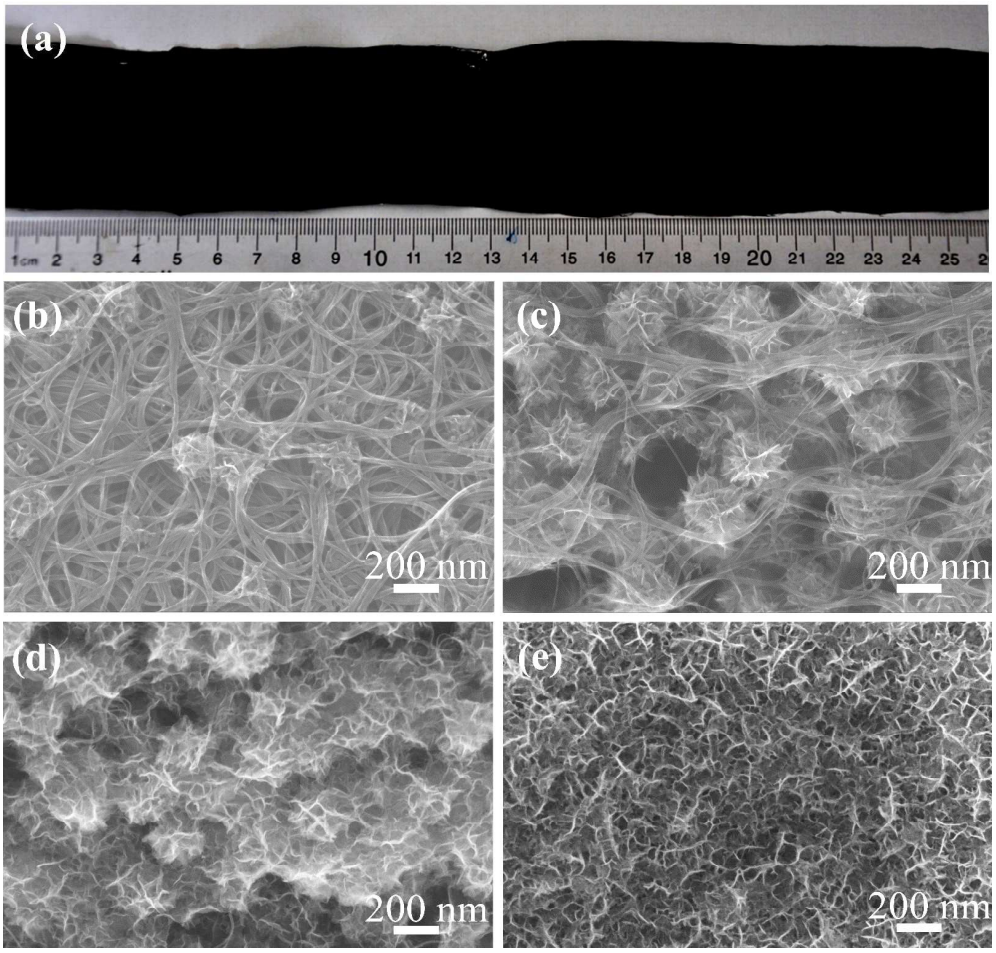

Fig. 1 (a) Optical image of a purified CNT macrofilm. SEM images of the CNT-MnO_x composite films prepared with deposition time of (b)100 s, (c)300 s, (d) 600 s, (e)1200 s.

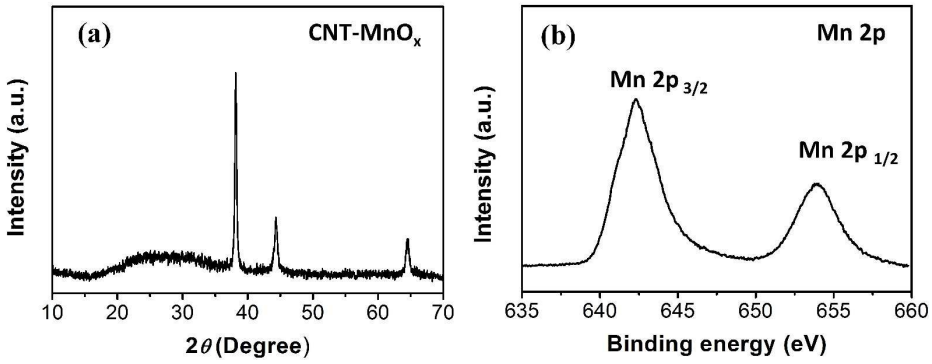

Fig. 2 (a) XRD pattern and (b) XPS spectrum of the CNT-MnO_x films prepared with deposition time of 1200 s.

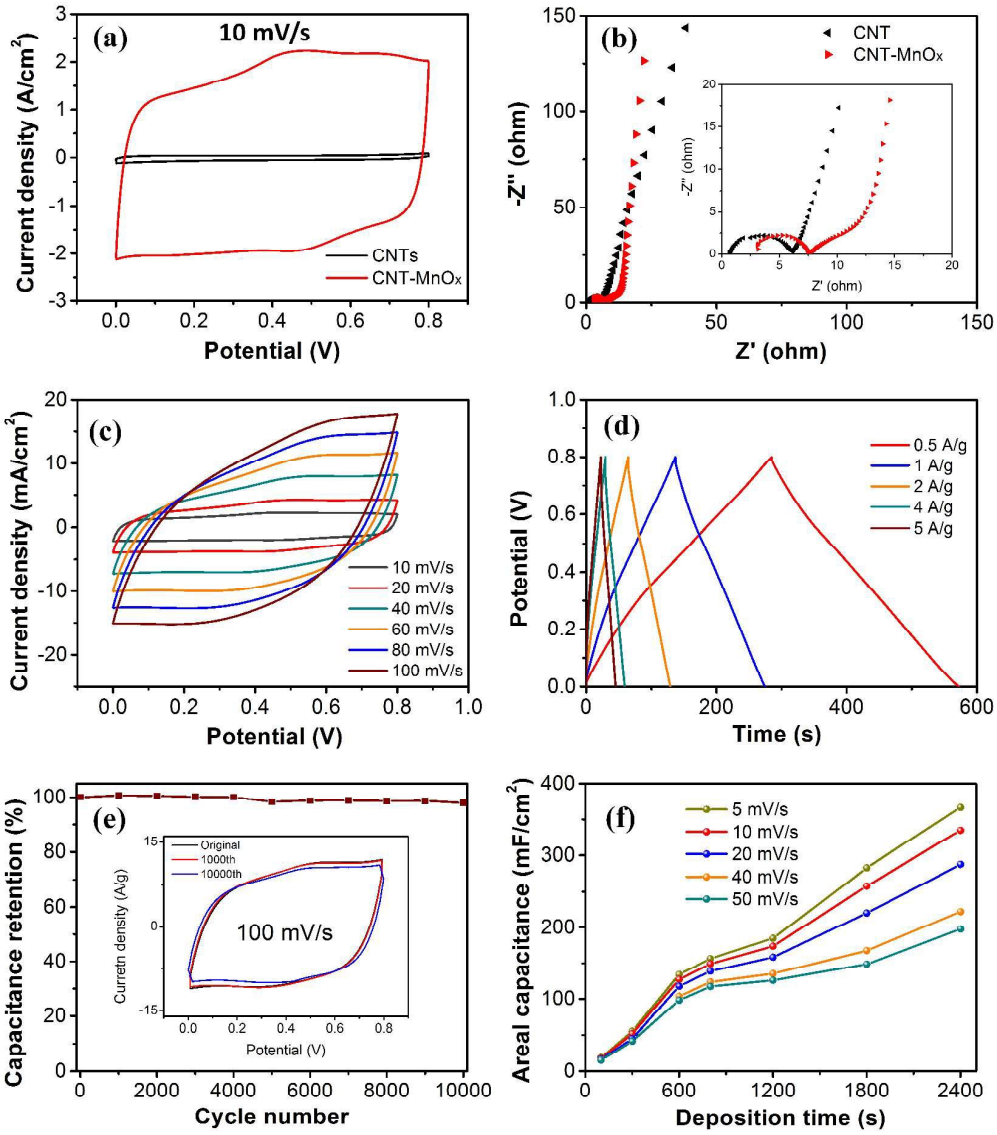

Fig. 3 Electrochemical properties of the purified CNT film and CNT-MnO_x composite film electrode (deposition time: 1200 s) in 0.5 M Na_2SO_4 aqueous solution electrolyte. (a) CV curves at 10 mV/s. (b) Nyquist curves of pure CNT and CNT-MnO_x composite. (c) CV curves at different scan rates. (d) GCD curves at current density ranging from 0.5 to 5 A/g. (e) Cyclic stability at 100 mV/s. (f) Areal capacitance depend on the deposition time at various scan rates.

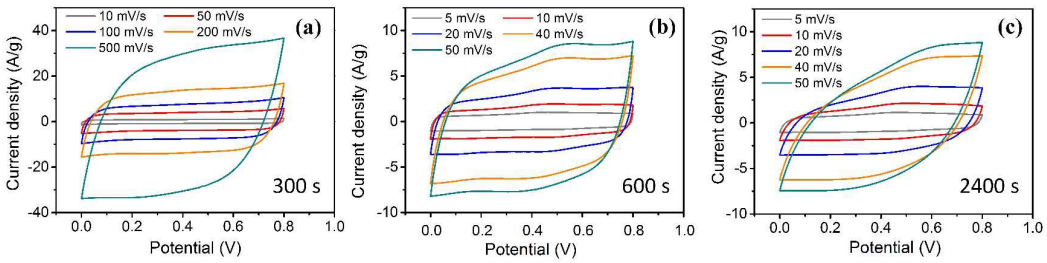

Fig. 4 CV curves at various scan rates of the CNT-MnO_x composite prepared at different deposition times. (a) 300 s, (b) 600 s, (c) 2400 s.

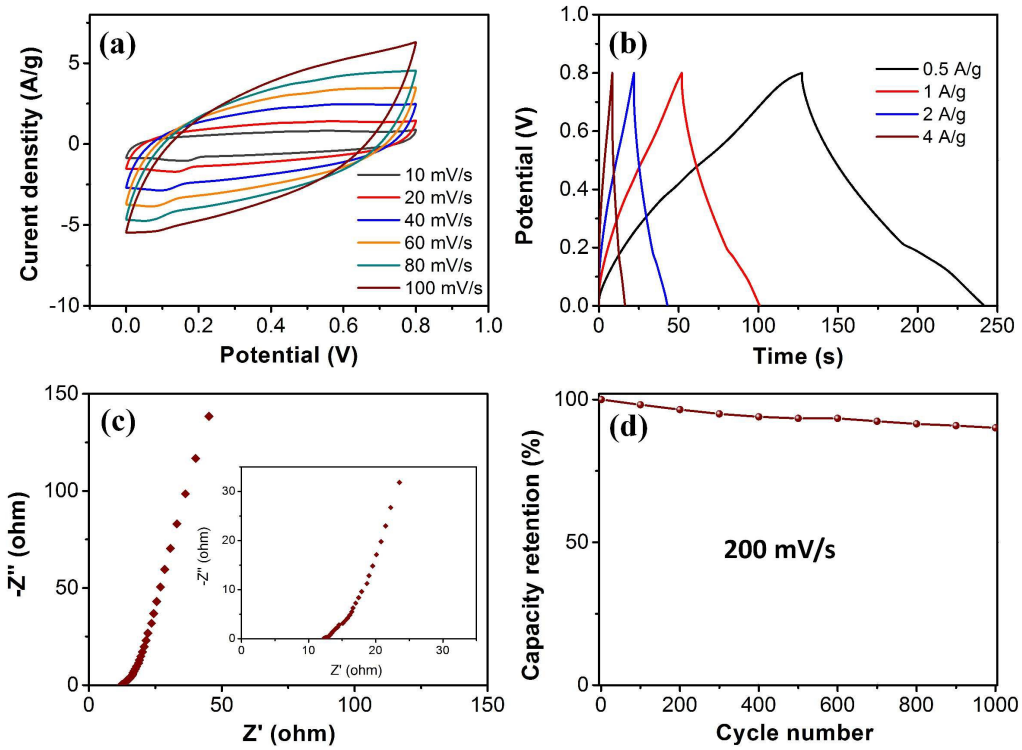

Fig. 5 Capacitive performance of the supercapacitors using CNT-MnO_x as electrodes (deposition time: 1200 s) and PVA-KOH as gel electrolyte. (a) CV curves at various scan rates. (b) GCD curves at current density ranging from 0.5 to 4 A/g. (c) Nyquist curves from 0.01 Hz to 100 KHz. Inset is the enlarged Nyquist curves. (d) Cyclic test at 200 mV/s for 1000 cycles.

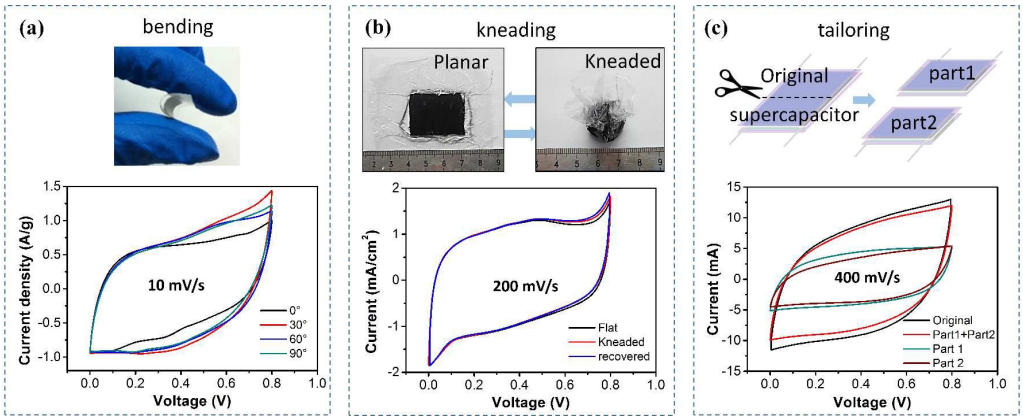

Fig. 6 Flexible and reliable behaviors of the CNT-MnO_x supercapacitor. (a) image and CV curves of a supercapacitor under bending to 30°, 60° and 90°. (b) Images and CV curves of supercapacitor with an area of 5 cm^2 on PE ceiling film under flat and kneading state. (c) CV curves of a supercapacitor before and after being cut into two parts. The schematic shows a supercapacitor being cut into two parts.

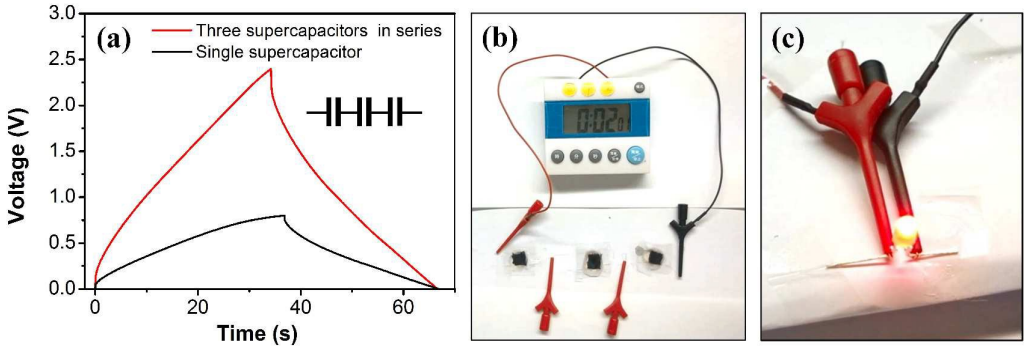

Fig. 7 Demonstration of application of the CNT-MnO_x supercapacitors. (a) GCD curves of an individual capacitor and three supercapacitors connected in series. Three supercapacitors in series (1 cm×1 cm) power a stopwatch (b) and a LED light (c).

Graphical Abstract

Highly flexible tailorable and all-solid-state supercapacitors are fabricated from the CNT-MnO_x composite films prepared by electrodepositing manganese oxide (MnO_x) to the carbon nanotube (CNT) macrofilms. The supercapacitors exhibit outstanding capacitive properties, high flexibility and reliability under bending, kneading and cutting.